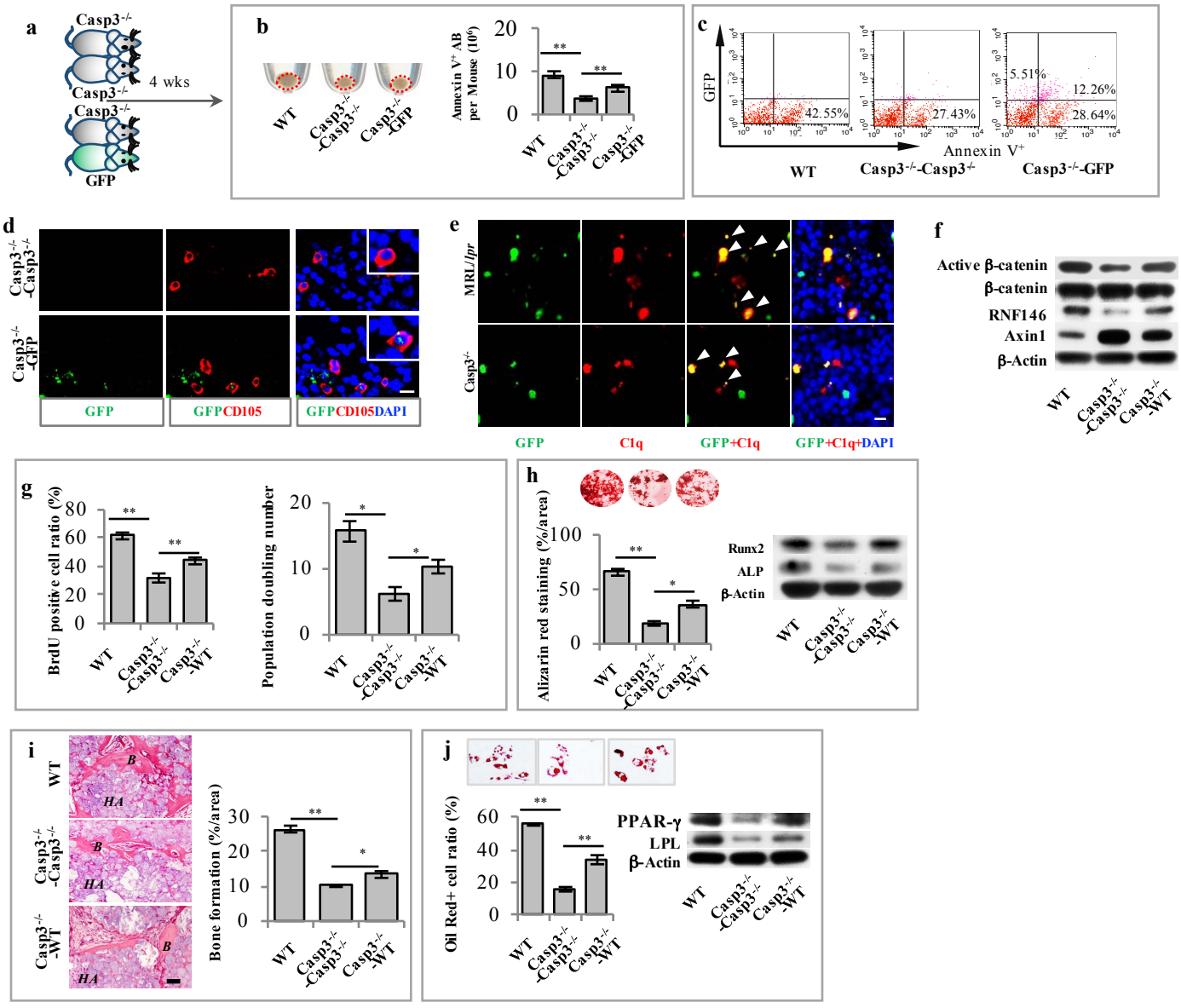

Supplementary Figure 7. Circulating apoptotic bodies rescued impaired MSCs in *Casp3*$^{-/-}$ mice. a, Scheme illustrating parabiosis approach. *Casp3*$^{-/-}$-*Casp3*$^{-/-}$, *Casp3*$^{-/-}$-GFP and *Casp3*$^{-/-}$-Wildtype (WT) parabiosis models were used. **b,** Compared to the control *Casp3*$^{-/-}$-*Casp3*$^{-/-}$ parabiosis model, the amount of apoptotic bodies was significantly increased in *Casp3*$^{-/-}$ mice in the *Casp3*$^{-/-}$-GFP parabiosis model. Flow cytometric analysis confirmed the elevated number of apoptotic bodies in the bone marrow of *Casp3*$^{-/-}$ mice from the *Casp3*$^{-/-}$-GFP parabiosis model. **c,** Flow cytometric analysis showed that GFP and Annexin V double-positive apoptotic bodies were detected in the bone marrow of *Casp3*$^{-/-}$ mice from the *Casp3*$^{-/-}$-GFP parabiosis model. The number of total Annexin V positive apoptotic bodies was increased in *Casp3*$^{-/-}$ mice from the *Casp3*$^{-/-}$-GFP parabiosis model. **d,** Immunofluorescent staining showed that CD105 positive cells in the bone marrow of *Casp3*$^{-/-}$ mice from the *Casp3*$^{-/-}$-GFP parabiosis model engulfed GFP apoptotic bodies. **e,** Immunofluorescent staining showed that most of the GFP signals detected in the bone marrow of MRL/*lpr* and *casp3*$^{-/-}$ were colocalized with apoptotic maker C1q (indicated by arrowhead). **f,** Western blot showed that the levels of RNF146 and active β-catenin were increased and the levels of Axin 1 were decreased in *Casp3*$^{-/-}$ MSCs from the *Casp3*$^{-/-}$-WT parabiosis model at 4 weeks post-parabiotic surgery. **g,** BrdU labeling and continued passage assay showed that *Casp3*$^{-/-}$ MSCs from the *Casp3*$^{-/-}$-WT parabiosis model had increased proliferation and population doubling rates compared to *Casp3*$^{-/-}$ MSCs from the *Casp3*$^{-/-}$-*Casp3*$^{-/-}$ parabiosis model. **h,** *Casp3*$^{-/-}$ MSCs from the *Casp3*$^{-/-}$-WT parabiosis model showed increased capacities to form mineralized nodules under the osteogenic inductive conditions, assessed by alizarin red staining (n = 5), and reduced expression of Runx2 and ALP, assessed by Western blot, when compared to *Casp3*$^{-/-}$ MSCs from the *Casp3*$^{-/-}$-*Casp3*$^{-/-}$ parabiosis model. **i,** *Casp3*$^{-/-}$ MSCs from the *Casp3*$^{-/-}$-WT parabiosis model showed increased capacities to form new bone when implanted into immunocompromised mice compared to *Casp3*$^{-/-}$ MSCs from the *Casp3*$^{-/-}$-*Casp3*$^{-/-}$ parabiosis model. **j,** *Casp3*$^{-/-}$ MSCs from the *Casp3*$^{-/-}$-WT parabiosis model showed increased capacities to differentiate into adipocytes under the adipogenic inductive conditions, as assessed by Oil red O staining (n = 5), and reduced expression of PPAR-γ and LPL, as assessed by Western blot, when compared to *Casp3*$^{-/-}$ MSCs from the *Casp3*$^{-/-}$-*Casp3*$^{-/-}$ parabiosis model. All results are representative of data generated in three independent experiments. Error bars represent the S.D. from the mean values. $^{**}P < 0.01$; $^{*}P < 0.05$. Scale bar, 10 μm (**d, e**), 50 μm (**i**).